journal

J. Am. Ceram. Soc., 88 [11] 3116–3124 (2005)
DOI: 10.1111/j.1551-2916.2005.00568.x

Measurement of the Thermophysical Properties of a Thermoplastic Ceramic Paste Across its Solidification Range Using Power-Compensated Differential Scanning Calorimeter

Dean A. Barker and D. Ian Wilson†

Department of Chemical Engineering, Cambridge, CB2 3RA U.K.

The specific heat capacity, thermal conductivity, and thermal diffusivity of a thermoplastic ceramic paste were investigated on a power-compensated, differential scanning calorimeter (DSC) using the heat capacity spectral analysis method developed by Merzlyakov and Schick for measuring these parameters on low thermal conductivity solids. The paste features an ultra-fine zinc oxide powder (a number-length mean diameter, $D_{1,0}$, of 85 nm) as the discrete phase, and a thermoplastic continuous phase comprising a blend of organic waxes with a melting range of ca. 30°–70°C. This paste is formulated with a solids loading of 50 vol% and is currently used in a novel continuous casting process to manufacture pharmaceutical products. The properties of the paste were investigated over a temperature range encompassing the melt and solid states, and for solid loadings from 0 to 70 vol%. The results compare favorably with those obtained using transient line source and transient plane methods.

I. Introduction

Knowledge of a material's thermal transport parameters is of crucial importance for the successful formation of ceramics and filled polymer systems where thermal treatment forms part of the processing route[1] or there is a requirement for specific thermal properties for the finished product; for example, electronics packaging and components.[3–7] The manufacture of products with controlled geometry can be achieved by continuous extrusion or casting as is widely practiced in the metals and polymer industries, or by molding followed by cooling of thermoplastic materials such as chocolate. Continuous casting of a thermoplastic solid–liquid paste to yield a solid product[8] is less common, but this route has been used recently to generate a controlled release drug-delivery device.[9]

This technology uses a paste comprising an ultra-fine[10] zinc oxide powder (Table I) with solids volume fraction, $\varphi_s = 0.50$ (50 vol%), and a mixture of organic waxes as the binder/continuous phase (see Table II). The casting operation involves cooling of the paste from ca. 70°C to room temperature. Optimization of this process via numerical modeling of the coupled momentum and heat transfer problem requires reliable estimates of the thermophysical parameters. This paper reports the use of a novel method for the rapid measurement of several thermophysical properties using small sample volumes in a power-compensated differential scanning calorimeter (DSC), for a ceramic paste with thermal transport properties significantly different from those reported by the method's developers. An investigation of the rheology of the paste under these conditions will be reported separately.

DSC is routinely used to study enthalpy changes and to estimate apparent heat capacities: the latter may be deduced by analysis of transient responses to stepwise temperature changes.[11] Merzlyakov and Schick[1] reported a technique for simultaneously measuring heat capacity and thermal conductivity using a frequency domain analysis of the temperature and heat flow responses returned by a power-compensated DSC. They demonstrated its efficacy using a series of polymer samples including polystyrene, polymethyl methacrylate, and epoxy resins 160 and 4173. Their technique requires small samples (typically 30 mg) and requires shorter acquisition times than standard methods based on transient plane or line sources. The thermal conductivity of the ZnO paste studied here is an order of magnitude greater than that of most polymers, so the aims of this study were to establish the applicability of Merzlyakov and Schick's method to these ceramic materials, to examine the validity of measuring these thermal parameters in the melt state, and to compare the values with data obtained using commercially available line and plane source devices.

A conventional scanning calorimetry analysis of the ceramic paste's individual and combined constituents was performed on a Perkin-Elmer Pyris 1 power-compensated DSC (PerkinElmer Life and Analytical Sciences Inc., Boston, MA), indicating the temperature domains and enthalpies associated with phase changes in the paste. Estimates of thermal conductivity, thermal diffusivity, and apparent specific heat capacity were obtained using two transient methods on this device: (i) A standard analysis of heat flow following a stepwise temperature change, calculated using the DSC manufacturer's StepScan[11,12] mode of operation. Direct integration of the resulting heat flow peak (stepwise integration method, SIM) gives an estimate of the apparent specific heat capacity. (ii) Using the method reported by Merzlyakov and Schick,[1] which yields both heat capacity and thermal conductivity data from which thermal diffusivity can be calculated. This method relies on heat capacity spectra (stepwise frequency method, SFM) to provide information on the time-dependent nature of the heat flux between the DSC furnace and the sample. These results are compared against data obtained with two commercial thermal characterization instruments, the *KD2 Thermal Properties Analyzer* (transient line source, TLS, Decagaon, Pullman, WA) and the *Hot Disk Thermal Constants Analyzer* (transient plane source, TPS, Thermal Instruments Limited, Aylesbury, U.K.), both of which yield thermal conductivity and diffusivity, and additionally for the Hot Disk, volumetric apparent heat capacity.

II. Materials and Methods

(1) ZnO Paste

The standard paste formulation comprised of a discrete phase (50 vol%) of ZnO powder (Univentures Public Company Limited, Pathumthani, Thailand) and a continuous phase that was a blend of two organic waxes (Danisco Ingredients Malaysia, Penang, Malaysia, and ICI Americas Inc., Wilmington, DE)

H. M. Jennings—contributing editor

Manuscript No. 20424. Received October 15, 2004; approved April 18, 2005.
Support for DAB provided by the Tertiary Education Commission, New Zealand.
†Author to whom correspondence should be addressed. e-mail: ian_wilson @cheng.cam.ac.uk

Table I. Particle Characterization for the ZnO Powder Obtained by Image Analysis of SEM Micrographs and Results From a Coulter LS230 Laser Diffraction Particle Size Analyzer† Using PIDS mode (Detection Range: 40–2 mm)

SEM	
Morphology	Regular hexagonal prisms
Aspect ratio	1.7 (±0.5)
Sphericity	0.9

Laser diffraction		
Parameter	Units	Value
$D_{1,0}$	nm	85
Mode	nm	60
Median	nm	70
Specific surface area	m^2/g	3100

†TABeckman Coulter Inc., Fullerton, CA. SEM, scanning electron microscope; PIDS, polarization intensity differential scattering.

that consisted of mainly mono- and diglycerides of fatty acids (see Table II). Paste preparation involved the following steps:

(1) The continuous phase components were melted in a Pyrex beaker placed in a water bath at approximately 80°C.

(2) The ZnO powder was added progressively to the melt while stirring, thereby ensuring, in so as far as possible, that the powder was wetted well by the continuous phase, while minimizing the entrainment of air. This process should produce a paste of even color and smooth texture.

(3) The paste melt was spread onto a dish in a layer approximately 1 cm thick, and was held in a vacuum oven at 80°C for 2–3 h to promote degassing of the paste. The paste was then removed from the oven and filled into a large syringe while still in the melt state, for dispensing or forming into the desired geometry.

(2) Stepwise DSC Methods

The stepwise DSC methods rely on the evolution of the sample's apparent heat capacity with time to an imposed change in temperature. This response is then analyzed in one of two ways, either by integration to yield the total heat flow and hence heat capacity, or by analysis of the heat capacity spectral response to find the thermal conductivity.

The program utility *StepScan* included with the installed version of Pyris software (version 3.81),[12] allows a programmed step in temperature to be imposed on the sample over a short but finite time interval, with the end of the step time defined by heat flow equilibration criteria. The benefits of this method are twofold: (i) integration of the heat flow from the start of the step until equilibrium is reached allows the calculation of the apparent heat capacity,[11] (ii) the time-dependent response to the programmed temperature step yields the thermal conductivity and diffusivity of the sample.[1]

Figure 1(a) shows an example of the sample heat flow and temperature response to six consecutive 1 K temperature steps, from 22° to 28°C. Each step starts with an initial heat flow impulse that decays to a steady-state value as the sample temperature approaches equilibrium. This is followed by further impulses as the subsequent temperature steps are imposed by software control. The baseline heat flow, obtained from an identical step program, but with empty sample pans in both the reference and sample furnaces, has already been subtracted from the total heat flow to obtain the corrected sample heat flow as illustrated in Fig. 1(b).

Table II. Formulation Description for $\varphi_s = 0.5$ ZnO Paste

Component	Volume fraction
ZnO	0.5
PEG 100 stearate	0.1
Mono- and diglycerides of fatty acids	0.4

(A) SIM: SIM yields an estimate of the heat capacity by integrating the heat flow peak over the step time interval. The peak area is defined as that area between the heat flow trace and a baseline drawn between consecutive steady-state heat flows; this is shown diagrammatically in Fig. 1(b). The large negative transient in the heat flow signal evident at the start of the program step is an artifact produced by the control software, which is discounted in the integral calculation. The accuracy of this technique was assessed by testing two sapphire standards (8.8 and 28.5 mg) over the temperature range used in the paste experiments (see Fig. 2), and shows good agreement with the literature values,[12] with correlation coefficient (R^2) values of 1.000 and 0.987 for the 8.8 and 28.5 mg references, respectively.

(B) SFM: Merzlyakov and Schick[1] provide a series of spreadsheet macros for the determination of thermal conductivity, λ, and specific heat capacity, C_p, for the method described below. The temperature was varied over the range 20°–80°C for the solids volume fraction $\varphi_s = 0.5$, and φ_s was varied from 0.0 to 0.70 at $T = 20.5$°C.

(C) Theoretical Basis: The SFM is based on the propagation characteristics of a heat pulse through a sample. In practice, a pulse is generated using a high scanning rate, of the order of 100 K/min. For a given geometry, the speed of propagation of the heat wave through the sample depends on the latter's thermal conductivity, the propagation speed being proportional to the thermal conductivity. The transient heat flux appears as an evolution in the apparent heat capacity, C_{app}, and is considered here as a complex apparent heat capacity that may be expressed as a function of frequency, ω, as described in the following equation:

$$C_{app}(\omega) = \frac{C_\alpha(\omega)}{1 - (i\omega/K_c)C_\alpha(\omega)} \tag{1}$$

where ω is a harmonic of the fundamental frequency, ω_0 is defined from the duration of the temperature step, K_c represents the effective thermal contact between the sample and the furnace, and C_α is the apparent heat capacity that would be measured at the sample's surface given perfect thermal contact with the furnace. The transient response is examined in the complex domain, with the programmed step change in temperature generating a corresponding heat flow response with in-phase (real) and out-of-phase (imaginary) components. The physical interpretation is that slow transients produce a change through the entire sample, and therefore appear undamped and real. High-frequency transients only produce a small change through the sample and therefore appear damped and complex; this is the relationship between the frequency response and the thermal conductivity. Explicitly, the heat flow signal is broken down into a series of harmonics of the fundamental frequency, ω_0,

$$C_{eff}(\omega) = \frac{A_{HF}}{A_q} = \frac{\sum_{i=1}^{n} HF_i \cos(\omega)t_i - i\sum_{i=1}^{n} HF_i \sin(\omega)t_i}{\sum_{i=1}^{n} q_i \cos(\omega)t_i - i\sum_{i=1}^{n} q_i \sin(\omega)t_i} \tag{2}$$

where $C_{eff}(\omega)$ is the effective heat capacity at frequency ω, A_{HF} is the heat flow rate amplitude, A_q is the heating rate amplitude, and q_i is the ith heating rate. Thermal diffusivities, κ, were computed from the heat capacity and thermal conductivity data using

$$\kappa = \frac{\lambda}{\rho C_p} \tag{3}$$

where ρ is the density.

(D) DSC Heat Capacity Calibration: Calibration parameters and the DSC transfer function must be established

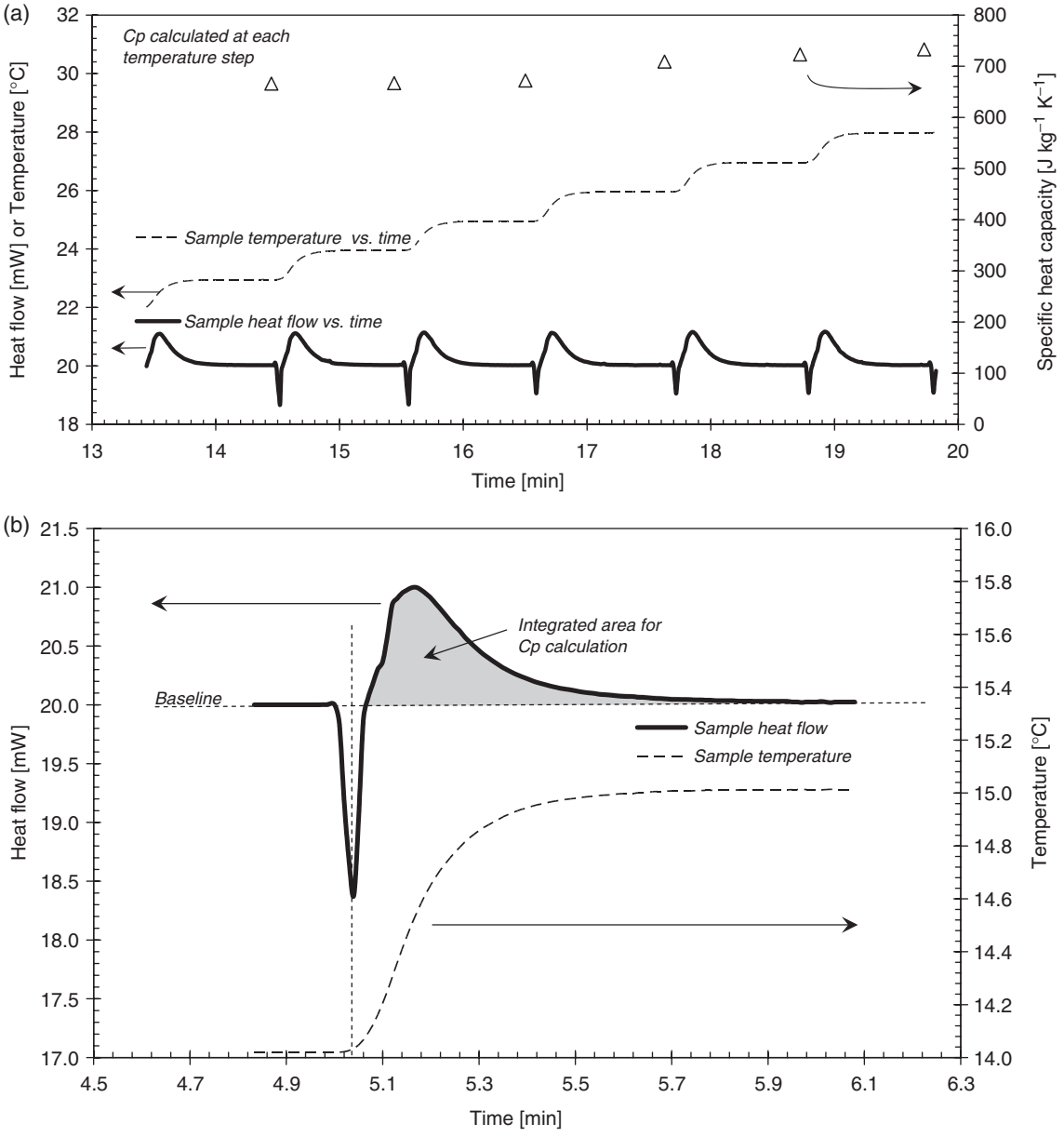

Fig. 1. (a) Example of the sample temperature, sample heat flow, and the calculated specific heat capacity using a Pyris 1 differential scanning calorimeter in the Stepwise mode of operation over six temperature steps for the $\varphi_s = 0.5$ ZnO paste. (b) An example of a single temperature step and the integration of the heat flow peak (shaded region) using the stepwise integration method technique.

before analyzing samples. This entails setting a test protocol (temperature step-profile) and then executing this profile for the baseline (sample and reference furnaces both empty), and then two times more with sapphire heat capacity standards (32.5 and 128.0 mg) preferably selected to bracket the expected sample mass. This process characterizes the DSCs transfer function, thereby allowing compensation of machine influences on the final heat flow trace.

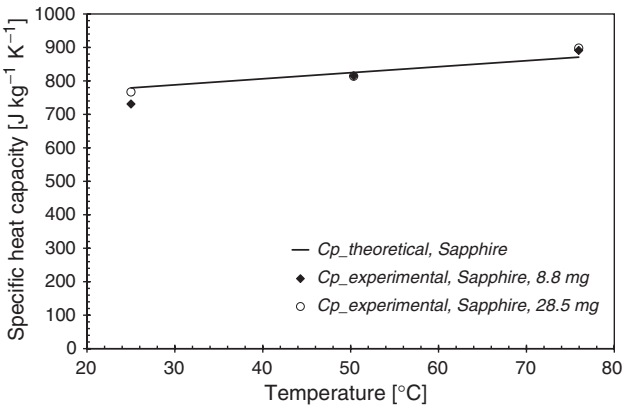

Fig. 2. Comparison of specific heat capacities of two sapphire references obtained using the stepwise integration method technique.

(E) Sample Preparation: Samples of the ZnO paste mix were prepared with volume ratios estimated from individual component densities at room temperature. The paste was then either placed in a 5 mL syringe for injecting into a 1 mL syringe for forming, or drawn directly into the 1 mL syringe if of sufficiently low viscosity (at $\varphi_s = 0$, 0.10, 0.20, and 0.30). The needle end of the 1 mL syringe had been removed so that the syringe barrel was of continuous internal diameter to allow for the extrusion of a solidified paste plug. The solidified plug was then ejected from the open end of the syringe, cut into small disks, and polished on a 25 μm (P600 grit) carborundum paper. This process yielded regular cylindrical samples typically 4.65 mm in diameter and between 1 and 2 mm thick.

The measured sample densities were similar to the predicted densities for φ_s values between 0 and 0.70, although the $\varphi_s = 0.70$ samples were not homogeneous because of the diffi-

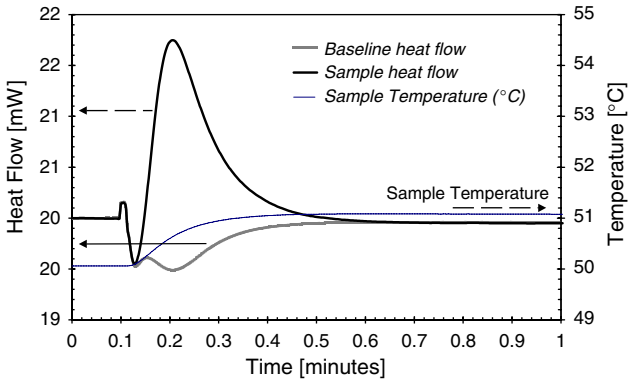

Fig. 3. Sample output for the $\varphi_s = 0.5$ ZnO paste sample showing heat flow and temperatures generated by a temperature step from 50.5° to 51.5°C at $t = 0.1$ min, followed by an isothermal stage.

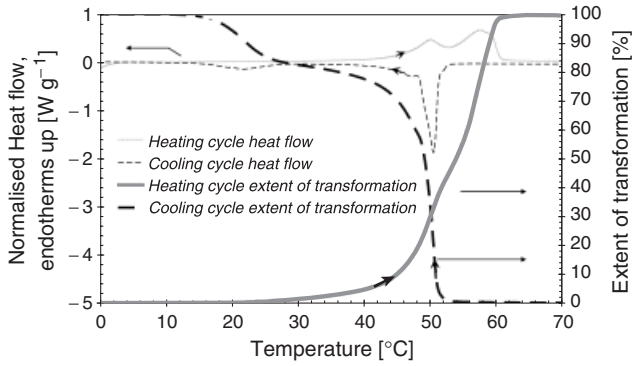

Fig. 5. Heating and cooling thermograms showing melting and solidification peaks and estimated extent of wax crystallization for $\varphi_s = 0.5$ ZnO paste.

culty in mixing the highly viscous paste obtained with this high solids loading.

An initial trial was conducted to gauge the effect of multiple heating and cooling cycles through the solidification transition on sample dimensions in order to ascertain whether it was possible to re-use samples. The samples' dimensions were found to be identical to their starting values (to within 0.025 mm) after cooling back to room temperature. However, slight erosion of the material at the perimeter of the face in contact with the furnace led to a small reduction in mass after each trial. For temperature dependency investigations, a single experimental sequence would generate data over the specified range of temperatures: the sample was left in place between temperature steps and the dimensions estimated using expansivity data obtained separately.

(F) An Illustration of Stepwise Data Analysis: The sample heat flow trace in Fig. 3 shows the typical data produced during a temperature step. The sample heat flow peaks 0.1 min after the stepwise temperature change is initiated (i.e., at 0.2 min) as the DSC control algorithm increases the heating rate to raise the sample temperature to that required by the program. The sample heat flow trace can be seen to decay exponentially after the peak, approaching a steady state after less than 0.5 min after the step was initiated. The sample temperature would match the programmed step change in temperature more closely if the sample thermal conductivity was larger, providing greater contributions to faster frequency components, and reduced contributions to slower frequency components for a given sample dimension and C_p. The frequency domain analysis generates plots such as those shown in Fig. 4, which indicate how well the model fits the experimental data. These particular data show a tendency to be localized on the left of the theoretical curve, suggesting that the heat wave propagated too quickly. A better result would have the data spread more evenly. This

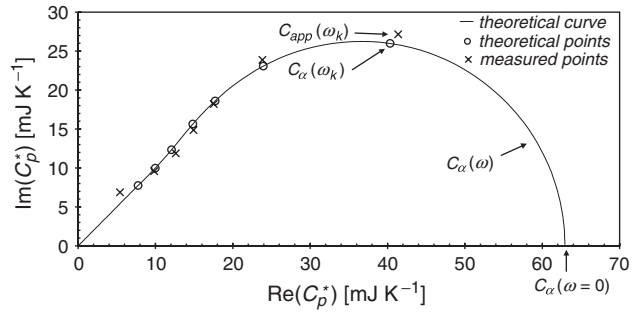

Fig. 4. Sample output from the data analysis of the $\varphi_s = 0.5$ ZnO paste, using the macros provided by Merzlyakov and Schick. This plot compares the fitted model points for the complex heat capacity C_p^*, (○), to the experimental points, (×).

adversely affects the estimation of the zero frequency (real) heat capacity, $C_\alpha(\omega = 0)$; a larger sample mass is advised in such cases.

Two programmed temperature step rates were used: 75 and 150 K/min. A better agreement between theoretical and experimental values of $C_\alpha(\omega)$ was observed with the higher step rate, and likewise for thicker specimens. Improvements were also observed by using a commercial heat sink paste (SMT Heat Sink Compound Plus, a metal oxide filled silicone oil paste from RS Components Ltd., Corby, U.K.) instead of the Apiezon® grease (M&I Materials Ltd., Manchester, U.K.) suggested by Merzlyakov and Schick. It should be noted that this method attempts to calculate the thermal contact resistance of the sample to the furnace via the heat transfer paste by using the initial transient data, rather than simply ignoring these points and only analyzing later data. It is possible that the errors were because of the relatively high thermal conductivity of the samples, but may also have been influenced by complex heat capacity behavior at lower temperatures where thermal analysis has subsequently shown phase changes occurring even close to room temperature (see Fig. 5); the underlying model assumes that the sample heat capacity is real and non-complex.

(3) TLS

The TLS technique analyzes the evolution of temperature at the probe/sample interface as a response to a known heat input. It differs in this respect from the complex heat capacity spectral analysis described in Section II*(1)(B)* in that the computational algorithm seeks a solution to an analytical expression for the heat conduction equation in the temporal domain.

The KD2 Thermal Properties Analyzer is a TLS probe consisting of a 0.9 mm diameter by 60 mm long stainless-steel needle, with a line heat source and temperature sensor embedded within. A micro-controller manages the power to the sensor's heating element and measures the probe temperature evolution, from which it computes the thermal conductivity and diffusivity. The device is able to measure thermal conductivities from 0.02 to 2 $W \cdot (m \cdot K)^{-1}$ and thermal diffusivities from 0.1 to 1.0×10^{-6} m^2/s. Measurements are straightforward, requiring that the probe be inserted into a hole in the sample primed with a heat transfer compound (here, Arctic Silver™ 3 Silver Polysynthetic Thermal Compound from Arctic Silver Inc., Visalia, CA). The test takes approximately 2 min for each temperature point.

(A) Theoretical Basis: The line source technique is based on an analytical solution for the heat conduction equation[13,14]; the temperature distribution for an unsteady line heat source in an infinite medium with initial temperature T_0 and cylindrical co-ordinates is given by

$$\Delta T(r,t) = T - T_0 = \left(\frac{q}{4\pi\lambda}\right) E_i\left(\frac{-r^2}{4\kappa t}\right) \quad (4)$$

where r is the radial position coordinate, q the heating rate per unit length, and E_i the exponential integral function

$$-E_i(-\chi) = \int_{\chi}^{\infty} \frac{1}{u}\exp(-u)\,du = -\gamma - \ln\chi - \sum_{n=1}^{\infty} \frac{(-1)^n \chi^n}{n!n} \quad (5)$$

where γ is Euler's constant. The higher order terms may be ignored for large t, yielding

$$T - T_0 \cong \frac{q}{4\pi\lambda}\left(\ln(t) - \gamma - \ln\left(\frac{r^2}{4\kappa}\right)\right) \quad (6)$$

where r is the distance between the line heat source and the temperature sensor.[14] When Eq. (6) is plotted against $\ln(t)$, $T(r, t)$ can be seen to exhibit a linear portion with slope $m = q/4\pi\lambda$ and intercept $n = m\ln(4\kappa/r^2\exp\gamma)$. The transport properties are then obtained from

$$\lambda \cong \frac{q}{4\pi m} \quad (7)$$

$$\kappa = \frac{r^2\exp\gamma}{4}\exp\left(\frac{n}{m}\right) \quad (8)$$

Heat capacity values were subsequently deduced from the diffusivity and conductivity data using Eq. (3).

(B) TLS Method: Approximately 0.20 L of the ZnO paste was formed in a glass beaker, where it was then degassed in a vacuum oven held at 80°C overnight. The beaker and sample were placed in a water bath connected to a temperature-controlled circulator for the entire duration of the experiment. Six holes marginally larger than the diameter of the probe were pre-formed in the solid sample and partially filled with the Arctic Silver™ 3 thermal transfer paste.

The desired system temperature was set on the circulator and the assembly was left to equilibrate for approximately 1 h. Several acquisitions were performed at each temperature, with successive readings taken after an equilibration period during which the sample temperature was monitored using the KD2's probe, and allowed to return to the initial temperature observed prior to the start of the test (a period of approximately 10 min). The relatively large sample mass meant that readings at successive temperatures required lengthy equilibration times, especially for those spanning the paste's phase change temperature regions. This extended equilibration requirement limited the number of results obtained during the available time. This apparatus does not allow for thermal contact resistance, preferring instead to minimize this effect by the use of thermal transfer paste at the probe/sample interface and by discounting the initial data most strongly influenced by the fast transients generated within the probe and the interfacial region. The ZnO paste lies at the upper limit of the range of thermal conductivities that can be measured using this device.

(4) TPS

In the TPS technique, a heat pulse is generated in a planar probe and the resulting time evolution of temperature is measured as a function of the probe resistivity; thus temperature sensing is not from a discrete component as it is for the TLS probe described in Section II*(3)*. The Hot Disk Thermal Constants Analyzer (Thermal Instruments Limited.) used consists of a spiral ohmic heating element of known electrical resistivity laminated between electrically insulating films. The sensor is sandwiched between two halves of the sample material to be tested. The response to a heat pulse is modeled by the heat conduction equation with the appropriate boundary conditions for this geometry, assuming an infinite sample medium. In practice, the sample size is chosen by specifying that the distance from any part of the sensor probe to the nearest outer surface of the sample must be greater than the probing depth, defined as $2(at)^{1/2}$, where t is the length of the test and a is the radius of the TPS sensor element.

Analysis of data from a TPS sensor probe may be described in terms of the temperature-dependent resistance of the heating element. The transient behavior of the temperature response may be described in a manner similar to that used for the TLS method described above. Similar regimes apply: the initial temperature increase is dominated by the temperature profile across the insulating laminate layer, while at longer times this will have relaxed and the temperature evolution is then dominated by the temperature change within the sample.

Data analysis first requires an iterative procedure to obtain κ for the sample before calculating λ. The TPS apparatus also aims to reduce the effects of contact resistance by ignoring the initial data points that tend to characterize the contact resistance rather than the sample's thermal transport properties.[15]

III. Results and Discussion

(1) Phase Change Behavior

The phase behavior of the solid-melt transition was initially explored using a Perkin-Elmer Pyris 1 DSC (PerkinElmer Life and Analytical Sciences Inc.) equipped with an Intracooler 2P for sub-ambient cooling to identify material properties such as glass transition temperatures, T_g, melting points, T_m, heats of melting or crystallization, ΔH, and heat capacities, C_p. This DSC is of a *power-compensated* type,[16] and uses two matched but separate low mass calorimeters or furnaces: one is used as the reference, while the other is used to hold the sample. Each furnace is maintained at the programmed temperature by independently controlled heating elements. The unit was calibrated for temperature, heat flow, peak area, and scan rate using indium and zinc references. Data analysis was conducted primarily on the Perkin-Elmer Pyris software (version 3.81).

Paste components were examined both individually and in combination. Samples were sealed in 50 μL aluminum pans fitted with perforated covers to eliminate isostatic pressure differences produced during testing. A variety of scans were undertaken to determine both rate and temperature dependence of the thermal features. The temperature program normally consisted of heating and cooling stages, each stage preceded by an isothermal equilibration period before the next program segment. Heating and cooling scan rates were varied between 0.5 and 100 K/min to test for rate-dependent effects, and then subsequently maintained at 20 K/min to assess the temperature-dependent properties. Scans generally commenced at 0°C and terminated at 80°C, thereby providing useful data over the range of approximately 10°–70°C. Repeated scans displayed little variation from one cycle to the next with this material, provided that a sufficient isothermal equilibration period was included prior to each heating/cooling cycle.

Figure 5 presents plots of the normalized heat flow recorded for the second run of a $\varphi_s = 0.5$ ZnO paste sample tested at 20 K/min. The multi-modal nature of the melting and solidification transitions is very evident, with a large separation evident in the cooling cycle between the first peak starting at 51.4°C and the second peak starting at 27.8°C. Table III summarizes the analysis of the data in Fig. 5, with the melting phase transition peaks analyzed as if they were one peak, but with the cooling peaks (at 51.4° and 27.8°C) analyzed in both combined and separate modes.

For the cooling cycle, the solidification onset temperature of the paste is 51.4°C. The first solidification peak (Peak 1 in Table III) is very sharp, and as indicated by the extent of transformation curve, with nearly 80% of the transformation (the solidification of the wax components) completed over a temperature interval of 10 K. A lower solidification peak (Peak 2 in Table III) is evident, with an onset temperature of 27.8°C. This peak was scanning rate dependent, its location moving to lower temperatures as the cooling rate increased, as illustrated by Fig. 6.

Table III. Summary of Melting and Solidification Temperatures and Enthalpy Changes for $\varphi_s = 0.5$ ZnO Paste

			Cooling		
Parameter	Units	Heating	Combined	Peak 1	Peak 2
Peak onset	°C	42.0	51.4	51.4	27.8
Peak end	°C	60.6	48.4	48.4	16.1
Peak maximum	°C	57.7	50.5	50.5	21.4
Peak height	W/g	0.65	−1.9	−1.8	−0.1
ΔH	J/g	19.8	−18.7	−14.1	−2.5

These results indicate that the melt viscosity is expected to be strongly temperature-dependent, with a sharp change in the viscosity over a 3 K interval (the main peak width given by the difference between the solidification peak onset and end temperatures). However, some extrudate plasticity can be expected to remain because of the remaining melt content, as there is a component of the solidification process that is slow and time-dependent. Figure 7(a) presents data from the individual paste components, the blend in the liquid phase, and the paste. The paste data are plotted as the heat flow trace divided by the mass fraction of the binder component as the ZnO does not contribute to any enthalpic changes in this temperature range, so that the *y*-axis represents the specific heat flow, in [W/g], of the continuous phase. The data analyses are summarized in Table IV.

An estimate of the expected total enthalpy change upon solidification based on a ratio of the individual components' mass contributions yielded values of $\Delta H = -122.7$ J/g for the blend, and −20.9 J/g for the $\varphi_s = 0.5$ ZnO paste system. This estimate is greater in magnitude than the measured value for the blend (−89.8 J/g), but additional experiments on the blend revealed the existence of a further crystallization event with an onset temperature of 4.0°C at this scanning rate, with $\Delta H = -22.7$ J/g. This accounts for some of the differences between the expected combined enthalpy changes on solidification for the blend, with the remaining difference probably being because of the original choice of baselines used for the area calculation to yield ΔH. Figure 7(b) shows a closer examination of the low-temperature solidification peak shown in Fig. 7(a) (centered at approximately 22°C), and reveals a possible source of the eutectic as the B component, which, in isolation, exhibits a similar peak at 32°C; the A component does not exhibit a solidification peak in this range. It is noteworthy that this secondary peak does not shift in the presence of ZnO.

The estimated value for the paste enthalpy change on solidification is −20.9 J/g compared with the experimental value of −18.7 J/g, representing a reasonable agreement—an error of approximately 10%—bearing in mind that the experimental value is underestimating the true value in the presence of still further enthalpic events that occur below room temperature at this scanning rate. Such estimates can therefore yield preliminary estimates of crystallization enthalpies for other solids volume fractions involving these paste components.

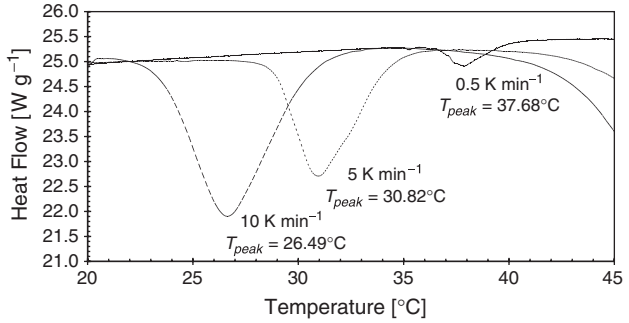

Fig. 6. Scanning rate dependency of the secondary peak for the binder blend cooled at 10, 5, and 0.5 K/min.

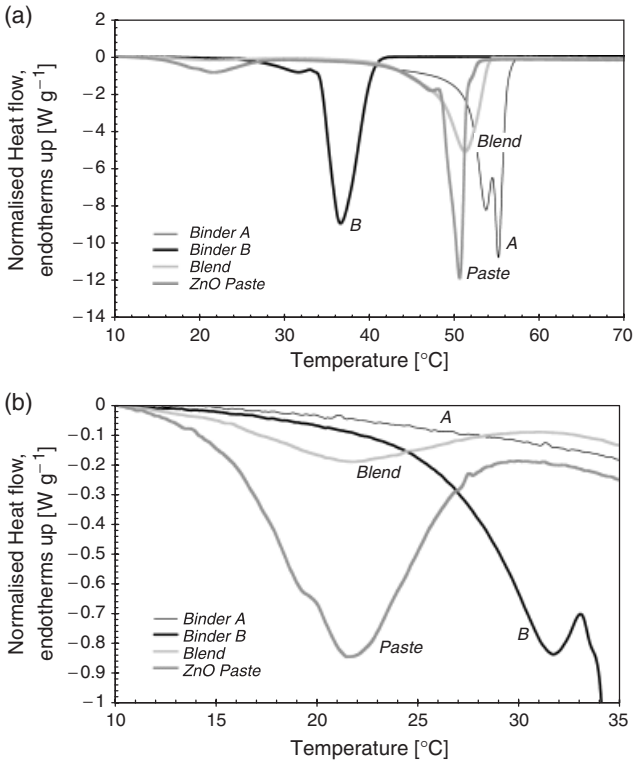

Fig. 7. (a) Heat flow contributions of the individual binder components A and B, the binder blend, and the paste (normalized) to the overall solidification profile, scanned by cooling at 20 K/min. (b) Paste constituent contributions to the secondary solidification peak scanned at 20 K/min.

The main binder component, A, has an onset temperature for solidification of 56.0°C, and the B component has an onset of 40.2°C; however, the blend starts to solidify at the intermediate value of 53.9°C with a broader solidification temperature range. This freezing point depression is consistent with the expected shift because of the mass ratios of the components in the blend. In the presence of ZnO powder, the onset decreases even further to 51.4°C, suggesting that the ZnO powder tends to delay solidification, at least at this volume fraction, which can be interpreted in terms of the effect of capillary size on solidification.[17]

(2) Specific Heat Capacity

Heat capacity values for the ZnO paste system were acquired for solids volume fractions in the range of $\varphi_s = 0$–0.7, and temperatures from 20° to 80°C.

(A) Effect of Solids Fraction on C_p: Data were acquired at the SFM technique with temperature step rates of 75 and 150 K/min at a temperature of 20.5°C, and are summarized in Fig. 8; error bars indicate the standard error in the measurements at

Table IV. Summary of Solidification Range Temperatures and Enthalpy Changes for Individual and Combined Paste Constituents for the $\varphi_s = 0.5$ ZnO Paste (not normalized)

Parameter	Units	Binder A	Binder B	Blend A+B	ZnO paste
Peak onset	°C	56.0	40.2	53.9	51.4
Peak end	°C	53.9	34.1	47.0	48.4
Peak maximum	°C	55.1	36.6	51.2	50.5
Peak height	W/g	−10.6	−8.9	−5.0	−1.9
ΔH	J/g	−123.7	−118.3	−89.8	−18.7

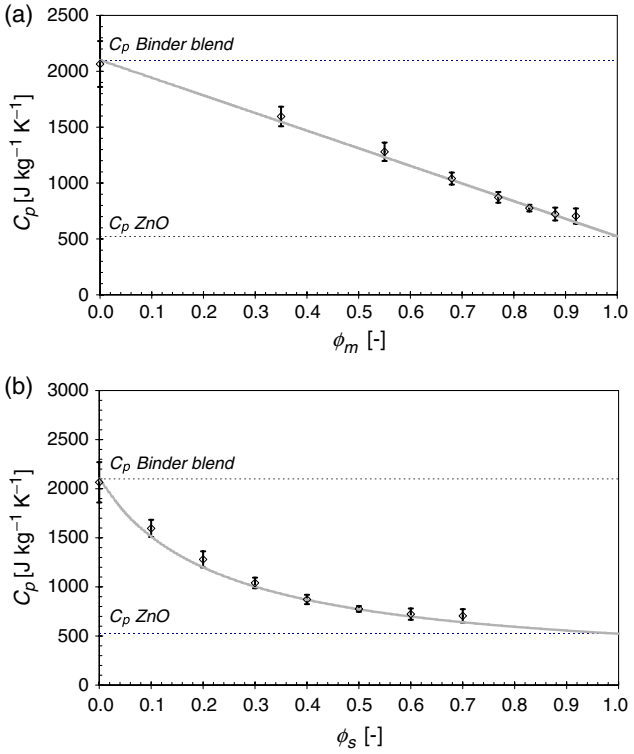

Fig. 8. (a) Specific heat capacity versus solids mass fraction, φ_m, at 20.5°C. Pure ZnO and binder heat capacities are indicated by horizontal dashed lines, and the solid line shows the simple linear mixing model given by Eq. (9). (b) An alternative plot of C_p versus solids volume fraction, φ_s, the gray line given by Eq. (10).

each value of φ_s. The limiting values for C_p are (i) for the binder only, $\varphi_s = 0$, $C_p = 2100\ \mathrm{J \cdot (kg \cdot K)^{-1}}$ for a typical organic wax similar to the binder used here,[18] and (ii) $C_p = 523\ \mathrm{J \cdot (kg \cdot K)^{-1}}$ for the ZnO powder.[18] These are indicated in Fig. 8 by horizontal dashed lines at their respective values.

The C_p value is strongly related to ZnO mass fraction as its density is approximately five times that of the binder. Figure 8(a) shows that a simple linear mixing rule holds for this material in terms of solids mass fraction, φ_m

$$C_p = 2100 + (523 - 2100)\varphi_m \quad R^2 = 0.932 \tag{9}$$

Figure 8(b) shows that C_p exhibits a non-linear decreasing dependency on φ_s, but this is also described by Eq. (10) with φ_m expressed in terms of φ_s, i.e., ideal mixing in terms of volumes, via.

$$C_p = 2100 + (523 - 2100)\frac{\varphi_s}{\varphi_s + 1050/5600(1 - \varphi_s)} \tag{10}$$

The slight deviation at higher solids loadings is attributed to the aforementioned lack of homogeneity in the paste at these values.

(B) Effect of Temperature on C_p: The apparent specific heat capacity of the ZnO paste system was studied at a single solids fraction, $\varphi_s = 0.50$, over the production process' temperature range including the melt state. Figure 9 shows data compiled using both SIM and SFM techniques and the TPS method. The SIM data were collected in both heating and cooling modes using 75 or 150 K/min. The analysis tools provided by Merzlyakov and Schick were unable to compute the results for λ within the phase change regions, as the model assumes that the signal does not contain complex components such as those produced by a phase change. However, it was possible to generate useable C_p results from the available data over the entire temperature range by restricting the analysis to the calculation of C_p. Both heating and cooling scans were used to investigate

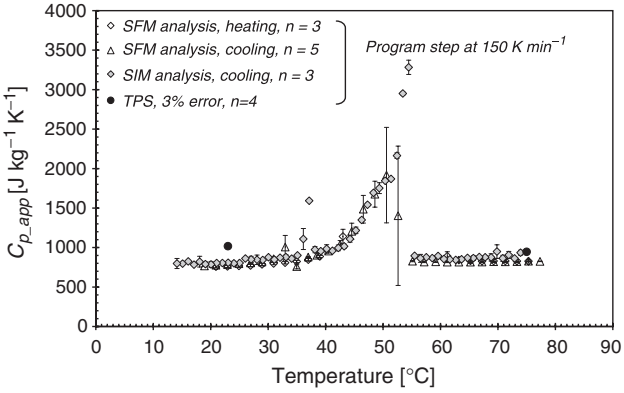

Fig. 9. Apparent specific heat capacity versus temperature for the $\varphi_s = 0.5$ ZnO paste using stepwise integration method (SIM), stepwise frequency method (SFM), and transient plane source (TPS). The error bars represent standard errors with the number of samples per datum, *n*, stated in the legend, with the exception of the TPS data where the error used is that stated in the literature.[15] The SIM and SFM analyses were conducted in heating and cooling modes to examine the possible existence of convective effects during the melt state when the sample is heated from below by the differential scanning calorimeter furnace.

whether there were any convection effects within the sample in the melt state. The SIM data for the phase change region in cooling mode are reported as there were differences between the melting and solidification characteristics (see DSC data in Fig. 5), and only the cooling segment is relevant to the process under consideration.

Figure 9 shows very good agreement among C_p values between the different methods. The SFM and SIM methods show an almost uniform value of approximately 880 $\mathrm{J \cdot (kg \cdot K)^{-1}}$ above and below the phase transition. The integrated temperature step results for temperatures within the solidification range were computed from programmed temperature steps followed by up to 5 min equilibration time to allow for complex heat evolution before commencing the next temperature interval. Only two temperature points were tested using the TPS method, 23° and 75°C, but each datum represents four experimental points. The TPS results at the higher temperature agree well with the DSC results, but the lower datum appears to be significantly higher. The reason for this variance is unknown, but there are two possible concerns: firstly, the TPS device yields values of volumetric heat capacity, which then have to be converted into specific heat capacity using an estimate for the density of the sample. The difference in densities, however, is unlikely to be attributable to a density effect. Secondly, data generated by the TPS method are weakly dependent on the test parameters, so it may be possible that these may require to be optimized further for this paste.

(3) Effect of Solids Fraction on Thermal Conductivity

Figure 10 presents λ values obtained for a number of samples over a range of solids fractions using the SFM method at heating rates of 75 and 150 K/min. Error bars were computed from the deviation between each calculated value of $C_\alpha(\omega_k)$ and the corresponding experimental value, $C_{app}(\omega_k)$. The λ value for the continuous phase agreed well with the literature values for similar organic waxes[18]; the value used was 0.29 $\mathrm{W \cdot (m \cdot K)^{-1}}$ (corresponding to the case, $\varphi_s = 0$), while the same source gave the thermal conductivity of the solid phase as 17 $\mathrm{W \cdot (m \cdot K)^{-1}}$. There appears to be a strong linear trend in thermal conductivity with $\lambda \propto \varphi_s$. This result is expected as the binder has a lower thermal conductivity than ZnO at this temperature and the increasing solids fraction will lead to an increasing network of pathways for improved heat conduction.

Three models were fitted to the data: (i) a series model, (ii) a parallel model, and (iii) the Maxwell model, which describes the

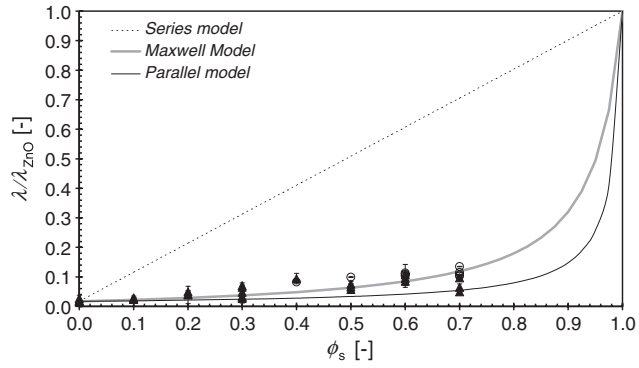

Fig. 10. Measured thermal conductivities at 20.5°C compared with the series model described by Eq. (11), the parallel model described by (12), and the Maxwell model for dilute spheres, described by Eq. (13). Error bars are calculated from the standard error in the samples at each volume fraction. (0, 75 K/min; ▲, 150 K/min.)

thermal conductivity of a dilute dispersion of spheres. The series model is described by[19]

$$\lambda_{mix} = \varphi_s\lambda_s + (1 - \varphi_s)\lambda_c \tag{11}$$

where λ_{mix}, λ_s, and λ_{cont} are the thermal conductivities of the mix, solid, and continuous phases, respectively. The parallel model is described by[19]

$$\lambda_{mix} = \frac{\lambda_s\lambda_c}{\varphi_s\lambda_c + (1 - \varphi_s)\lambda_s} \tag{12}$$

The Maxwell model[20] was also applied using

$$\lambda_{mix} = \frac{\lambda_s[(\lambda_s + 2\lambda_{cont}) - 2\varphi_s(\lambda_{cont} - \lambda_s)]}{(\lambda_s + 2\lambda_{cont}) + \varphi_s(\lambda_{cont} - \lambda_s)} \tag{13}$$

The models and data are plotted on Fig. 10, which indicates that the best overall representation is given by the Maxwell model with the ZnO as the dispersed phase, although this is intended for dilute dispersions of spheres. This model is able to describe the thermal conductivity of higher solids loadings, but fractions above 0.7 are unlikely to be used for an extrudable paste formulation.

(4) Effect of Temperature on λ and κ

The thermal characteristics of the ZnO paste system with $\varphi_s = 0.50$ were studied over the production process temperature range including the melt state.

The thermal conductivity data in Fig. 11 show the results calculated from SFM, TLS, and TPS methods. There is a variation greater than that observed with C_p, with larger error bars for the SFM values. The TLS method yielded values lower than those of the other methods, and required long data acquisition times resulting from the sample's relatively large thermal mass associated with the 60 mm long probe. The TLS result at 44°C shows the effect of non-ideal conditions on the apparent thermal conductivity, in this case arising from latent heat effects. Note that the error bars for this datum describe the range of the values measured after an equilibration period (ca. 30 min). The plot indicates that there is little difference in thermal conductivity either side of the solidification temperature range, with a value of approximately 1.9 $W \cdot (m \cdot K)^{-1}$ in the melt region above 55°C, and approximately 2.1 $W \cdot (m \cdot K)^{-1}$ below 37°C.

The thermal diffusivity data presented in Fig. 12 were calculated either from C_p and λ results from the SFM method, or were obtained directly by the TPS and TLS methods. The trend in the SFM results is not as clear for this parameter as they were for previous C_p and λ results, in part because of the compounding nature of the errors associated with this computed value. The data scatter and resulting error bars are large, especially below the solidification temperature range. This reflects the quality of the original data where the thermal conductivity results in this temperature range displayed greater scatter than the results for the melt state, again possibly influenced by further enthalpic events at these lower temperatures. Conversely, the TLS results display good agreement with the TPS results, suggesting that the SFM diffusivity results may be too high. This would be consistent with the apparent C_p values for the DSC data being low, as suggested in Fig. 9. With this taken into consideration, it is possible to specify the thermal diffusivity for two regions; one for above the onset of solidification and one below. This would suggest a thermal diffusivity of approximately 8×10^{-7} m^2/s above 55°C and 1×10^{-6} m^2/s below 55°C.

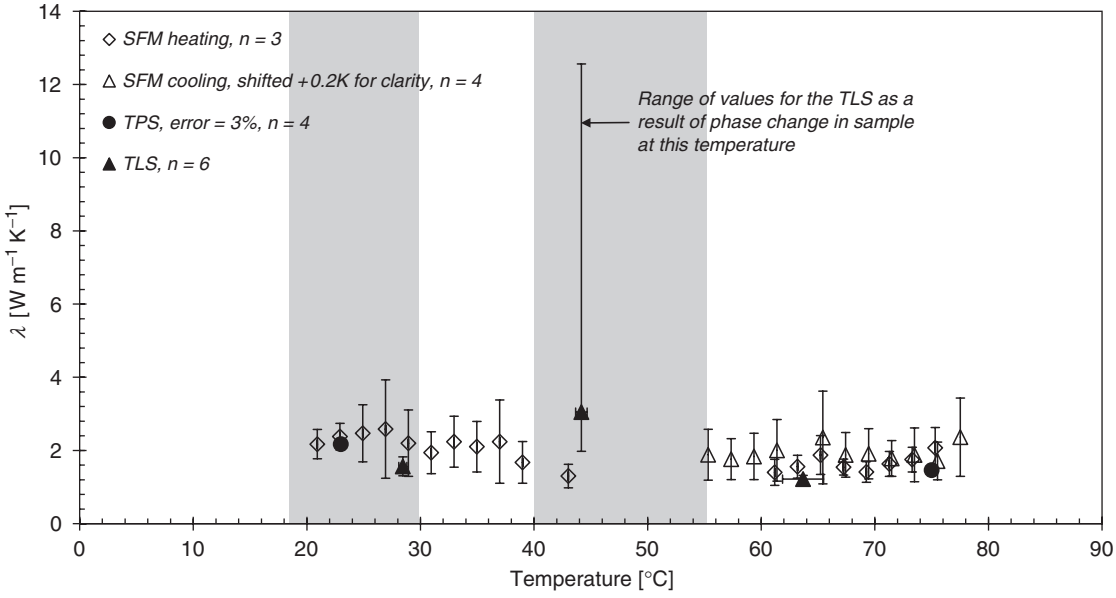

Fig. 11. Thermal conductivity, λ, versus temperature for a ZnO paste, $\varphi_s = 0.50$. Error bars are calculated from the "deviation" parameter calculated by the analysis spreadsheet for the stepwise frequency method (SFM) results, and from the standard errors for the transient plane source (TPS) and transient line source (TLS) results, with the exception of the TLS value at 44°C where the range of values is shown. The number of repetitions for each method is denoted in the legend by "*n*". The TPS method error bars show a 3% error as described in the literature.[15] The shaded regions show temperatures at which phase changes (producing a complex apparent heat capacity) may be influencing the accuracy and validity of the results.

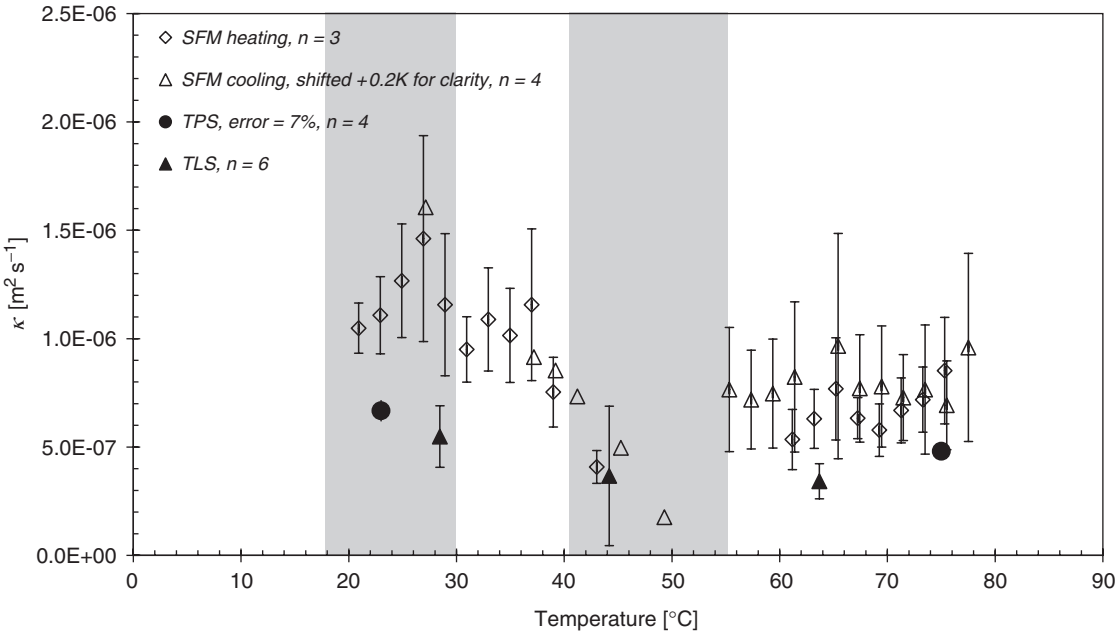

Fig. 12. Thermal diffusivity, κ, versus temperature for the $\varphi_s = 0.5$ ZnO paste by transient plane and line source methods using stepwise frequency method (SFM), transient plane source (TPS), and transient line source (TLS) apparatuses. The error bars represent standard errors with the number of samples per datum, *n*, stated in the legend, with the exception of the TPS data, where the error used is 7% as described in the literature.[15] The shaded regions show temperatures at which phase changes (producing a complex apparent heat capacity) may be influencing the accuracy and validity of the results.

This study has demonstrated that power-compensated DSC can be used to obtain thermal transport properties in an efficient manner, with very small samples, and over wide temperature ranges. Most temperature steps only take approximately 30 s to execute, so after the calibration runs have been completed, the sample baseline and actual sample runs should take approximately 1 min to acquire for each temperature point. Merzlyakov and Schick's calculation routines take time to compute, but this task is relatively quick on a modern PC. If more complex features such as phase change occur during testing, the thermal conductivity analysis will most likely fail to converge, but an alternative analysis selection confines the computation to the apparent specific heat capacity, which will then most likely yield a result.

IV. Conclusions

Standard DSC analysis, stepwise DSC analysis, and TLS and plane source techniques were used to characterize the individual and combined constituents of a thermoplastic paste formulation. These methods yielded detailed data on the paste's enthalpy changes, specific heat capacity, thermal conductivity, and thermal diffusivity for a range of solids fractions from $\varphi_s = 0$ to 0.70, and temperatures from 20° to 80°C. The results were found to be in good agreement with the literature values where available, and were otherwise in relatively good agreement across the different methods.

In this work, we have shown the efficacy of the stepwise DSC techniques for the study of a ceramic paste's thermal transport properties on small samples (of the order of several millimeters in size), for thermal conductivities up to approximately 2.5 $W \cdot (m \cdot K)^{-1}$, for both the melt and solid states. These data were required for a numerical simulation of the thermal processing method required for this particular material, but the methods described offer significant utility to anyone requiring data for similar paste, ceramic, or other highly filled systems.

Acknowledgments

We wish to acknowledge laboratory support from Zlatko Saračević (Department of Chemical Engineering, University of Cambridge); technical support from Paul Clarke, Paul Gabbott, and Conrad Seccombe from PETA Solutions/PerkinElmer Inc.; HotDisk testing by Dr. Richard Seddon from MERL, U.K., and access to the KD2 device at the Department of Chemical Engineering and Chemical Technology, Imperial College London, courtesy of Dr. Frantisek Štěpánek. Materials were kindly donated by The Horticultural and Food Research Institute of New Zealand Limited.

References

[1]M. Merzlyakov and C. Schick, "Thermal Conductivity from Dynamic Response of DSC," *Thermochim. Acta*, **377** (1–2), 183–91 (2001).
[2]B. Weidenfeller, M. Hofer, and F. R. Schilling, "Cooling Behaviour of Particle Filled Polypropylene During Injection Moulding Process," *Compos. Pt. A-Appl. Sci. Manuf.*, **36**, 3 (2005).
[3]B. Weidenfeller, M. Hofer, and F. Schilling, "Thermal and Electrical Properties of Magnetite Filled Polymers," *Compos. Pt. A-Appl. Sci. Manuf.*, **33**, 8 (2002).
[4]Yi He, "Heat Capacity, Thermal Conductivity, and Thermal Expansion of Barium Titanate-Based Ceramics," *Thermochim. Acta*, **419**, 1–2 (2004).
[5]C. P. Wong and R. S. Bollampally, "Thermal Conductivity, Elastic Modulus, and Coefficient of Thermal Expansion of Polymer Composites Filled With Ceramic Particles for Electronic Packaging," *J. Appl. Polym. Sci.*, **74**, 14 (1999).
[6]L. Kehoe, P. V. Kelly, G. M. O'Connor, M. O'Reilly, and G. M. Crean, "A Methodology for Laser-Based Thermal Diffusivity Measurement of Advanced Multichip Module Ceramic Materials," *IEEE Trans Compon. Packag. Manuf. Technol. Pt. A*, **18**, 4 (1995).
[7]D. M. Liu, "Thermal-Diffusivity, Specific-Heat, and Thermal-Conductivity Of $(Ca_{1-x},Mg_x)Zr_4(Po_4)_6$ Ceramic," *Mater. Sci. Eng. B-Solid State Mater. Adv. Technol.*, **23**, 2 (1994).
[8]R. M. McDonald, Patent No. NZ Patent 294951 (October 1997).
[9]R. Munday, Patent No. US Patent 5720972 (March 1996).
[10]C. Rauwendaal, *Polymer Extrusion*, 3rd edition, Hanser, Munich, 1994.
[11]B Cassel, *A Stepwise Specific Heat Technique for Dynamic DSC*. Perkin-Elmer Life and Analytical Sciences Inc., Boston, MA, 2000.
[12]Perkin-Elmer Inc., *Pyris Software for Windows, ver. 3.81*. Perkin-Elmer Life and Analytical Sciences Inc., Boston, MA, 1999.
[13]Decagon Devices Inc., *KD2 User's Manual version 1.0 Thermal Properties Analyzer*. Decagon Devices Inc, Pullman, WA, 2001.
[14]Decagon Devices Inc., "Using Thermal Properties Measurements to Predict Food Temperature During Processing,"Application Note, Washington, 1999.
[15]S. E. Gustafsson, "Transient Plane Source Techniques for Thermal-Conductivity and Thermal-Diffusivity Measurements of Solid Materials," *Rev. Sci. Instrum.*, **62**, 3 (1991).
[16]W. J. Sichina, *Benefits and Applications of the Power Compensated Pyris 1 DSC*. PerkinElmer Life and Analytical Sciences Inc., Boston, MA, 2000.
[17]C. L. Jackson and G. B. McKenna, "The Melting Behavior of Organic Materials Confined in Porous Solids," *J. Chem. Phys.*, **93**, 12 (1990).
[18]H. P. R. Frederikse and R. Lide David, *CRC Handbook of Chemistry and Physics*, 77th edition, CRC Press, Boca Raton, FL, 1996.
[19]J. E. Parrott and D. Audrey Stuckes, *Thermal Conductivity of Solids*. Pion, London, 1975.
[20]M. J. Morley and C. A. Miles, "Modelling the Thermal Conductivity of Starch-Water Gels," *J. Food Eng.*, **33**, 1–2 (1997). □